minerals

MDPI

Article

Spatiotemporal Evolution of Central Qilian Shan (Northwest China) Constrained by Fission-Track Ages of Detrital Grains from the Huangshui River

Xu Lin [1,2,*], Marc Jolivet [3,*] and Feng Cheng [4]

[1] College of Civil Engineering and Architecture, China Three Gorges University, Yichang 443002, China
[2] Key Laboratory of Geological Hazards on Three Gorges Reservoir Area, Ministry of Education, China Three Gorges University, Yichang 443002, China
[3] Géosciences Rennes–UMR CNRS 6118, Université de Rennes, 35000 Rennes, France
[4] School of Earth and Space Sciences, Peking University, Beijing 100871, China; chengfeng@pku.edu.cn
* Correspondence: hanwuji-life@163.com (X.L.); marc.jolivet@univ-rennes1.fr (M.J.)

Abstract: The emergence of the Tibetan Plateau is one of the most significant geological events in East Asia. The Central Qilian Shan connects North and South Qilian Shan in the northeastern part of the Tibetan Plateau. However, the exhumation history of the Central Qilian Block from the Mesozoic to Cenozoic remains unclear. Determining the cooling ages of detrital zircon and apatite in modern river sediments is an ideal method for tracing the evolutionary processes of orogenic belts. In this study, we present the first single-grain detrital apatite (153) and zircon fission-track (108) data for the Huangshui River sediments from the Central Qilian Shan. The decomposition of the dataset revealed major Mesozoic and Cenozoic age peaks at ca. 145–93, and 11 Ma. The Central Qilian Shan entered the intracontinental orogeny stage dating back to the Cretaceous (ca. 145–93 Ma) and Late Cenozoic (ca. 11 Ma) caused by the subduction of the Neo-Tethys and Indian–Asian collision. Therefore, we propose that the geomorphic framework of the northeastern margin of the Tibetan Plateau was initially established during the Mesozoic and further consolidated in the Late Miocene.

Keywords: Central Qilian Shan; Huangshui River; detrital zircon; fission track; LA-ICP-MS; Tibetan Plateau

Citation: Lin, X.; Jolivet, M.; Cheng, F. Spatiotemporal Evolution of Central Qilian Shan (Northwest China) Constrained by Fission-Track Ages of Detrital Grains from the Huangshui River. *Minerals* **2023**, *13*, 890. https://doi.org/10.3390/min13070890

Academic Editor: Giovanni Mongelli

Received: 21 May 2023
Revised: 21 June 2023
Accepted: 27 June 2023
Published: 30 June 2023

1. Introduction

The emergence of the Tibetan Plateau is one of the most significant geological events in East Asia [1–6] (Figure 1a). However, its details remain unclear. Two main evolutionary models have been proposed for the Tibetan Plateau: (a) since the Early Cenozoic, the Tibetan Plateau has experienced a gradual uplift from south to north and the geomorphic boundary of the northeastern margin of the plateau appeared in the Pliocene [7,8]; and (b) the rise of the northeastern Tibetan Plateau synchronously coincided with the India–Eurasia collision to the south, which started in the Cenozoic [1,9]. The biggest difference between the two models is the emergence time of the northeastern margin of the Tibetan Plateau. Therefore, further research is needed to provide insights into the evolution of the Tibetan Plateau.

The 800 km long Qilian Shan along the northernmost margin of the Tibetan Plateau (Figure 1b) is an excellent location to study the formation of the Tibetan Plateau [9–14]. It has experienced multiple episodes of tectonic deformation due to continental convergence, oceanic opening and subduction, and intracontinental orogeny [15,16], recording the initial appearance of the geomorphic boundary in the northeastern Tibetan Plateau [9,10,17]. The Central Qilian Shan connects the North Qilian Shan and South Qilian Shan (Figure 1b), which is important for understanding the evolutionary processes of the entire Qilian orogenic belt [18–21].

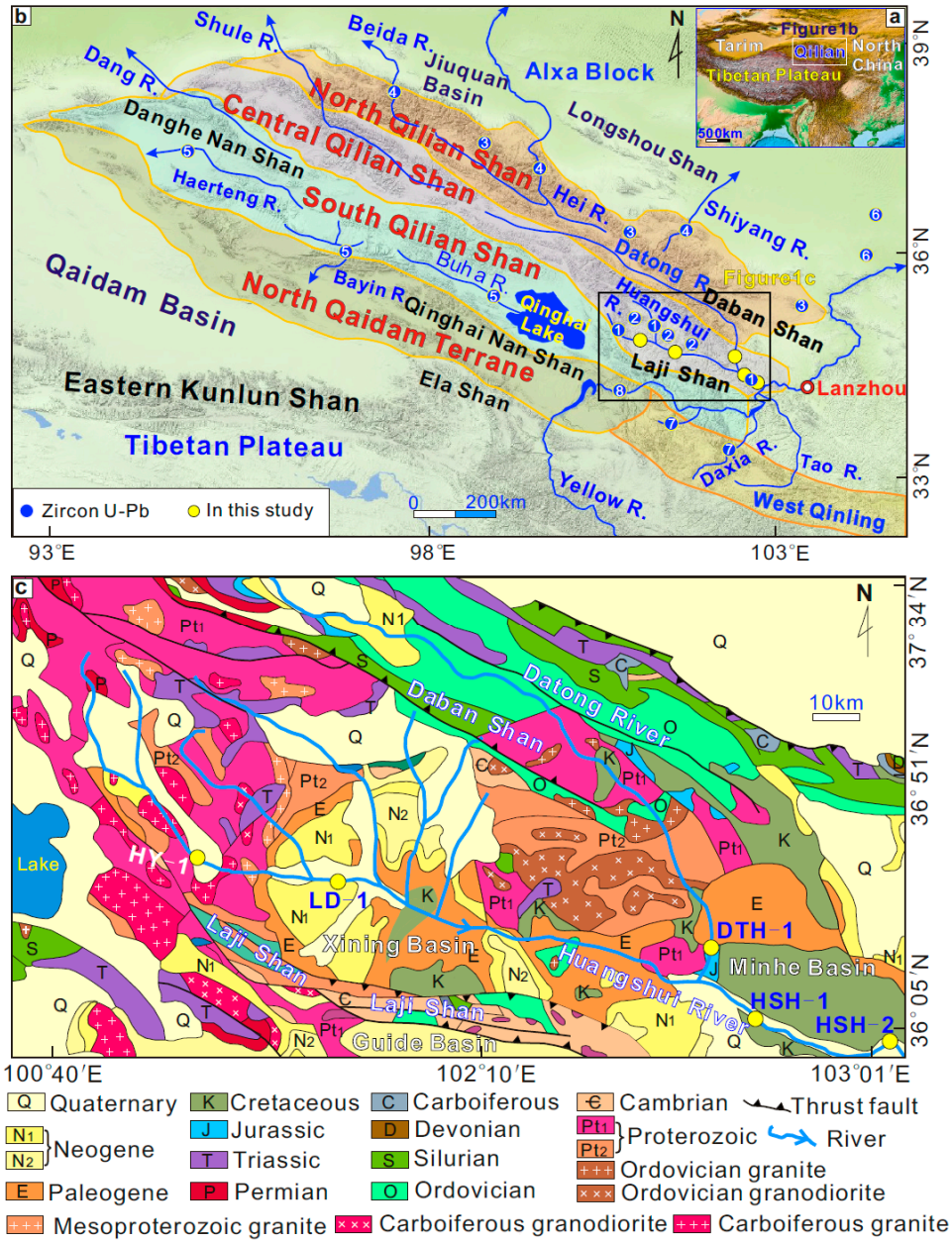

Figure 1. (**a**) Map showing the location of the Qilian Shan. (**b**) Tectonic units of the Qilian orogenic belt including sampling locations from this and previous studies. Zircon U-Pb ages are from the following references: (1) [22,23]; (2) [24]; (3) [25,26]; (4) [27,28]; (5) [29,30]; (6) [26]; (7) [31]; (8) [32]. (**c**) The geological map of the catchment of the Huangshui River following the 1:2.5 million scale geologic map of China (modified from [33]).

The U–Pb age reflects the time of zircon crystallization at >700 °C and can be used to identify the grain provenance from the comparison between bedrock and detrital ages [22]. It has been widely used to study the early tectonic evolution of the Central Qilian orogenic belt [11,34–37]. In contrast, the fission-track ages of zircon (ZFT) and apatite (AFT) are low-temperature thermochronometric data that are sensitive to temperatures ranging from 240 to 60 °C [9,38], recording the exhumation of the orogenic belt in a later period. Therefore, they are commonly used to investigate the thermal history of the Central Qilian Shan. For example, bedrock AFT results revealed that the initiation of uplift in the Central Qilian Shan occurred between 17 and 13 Ma [39–41]. However, other authors have used bedrock AFT and ZFT analyses to describe the rapid cooling of the Central Qilian Shan since the Cretaceous [18,42–44]. In addition, Zuza et al. [19] reported the FT and (U–Th)/He ages of

bedrock apatite and zircon from the Central Qilian Shan, suggesting that the exhumation was initiated between 40 and 35 Ma. As the response times of different locations of the bedrock's orogenic belt to the same tectonic event are inconsistent, such crustal sections may be completely eroded or may partly record the thermal history over time. Therefore, the exhumation times of the Central Qilian Shan remain controversial.

As sediments are primarily transported by rivers from the orogen to the basins, collecting samples from modern river sediments holds great potential for determining the long-term evolutionary history of orogenic belts [45–50]. Detrital zircon and apatite grains are accessory minerals that are abundant in river sediments and are well-established tools for studying the long-term exhumation history of the southern [51] and western Tibetan Plateau [52]. However, there is a lack of this type of research in the Central Qilian Shan (NE Tibetan Plateau) (Figure 1c). Therefore, we conducted FT dating of modern fluvial detrital zircon and apatite in the eastern parts of the Central Qilian Shan for the first time to discuss its thermal history.

2. Geological Setting

2.1. Qilian Shan

The Qilian Shan between the Tarim Craton, North China Craton, and Qaidam Block defines the modern northeastern boundary of the Tibetan Plateau (Figure 1a). Based on the location of the suture zone, the Qilian orogenic belt can be divided into three parts from north to south: the North Qilian Shan, the Central Qilian Shan, and the South Qilian Shan [1,15,16] (Figure 1b). The entire Qilian Shan was reactivated by thrusting that began during the Cretaceous along the Hexi Corridor to the north and the North Qaidam terrane to the south [8,53–55] (Figure 2a,b). The Qilian orogenic belt has undergone a significant lateral expansion and vertical uplift due to the far-field effect of the collision between India and Eurasia since the Cenozoic [56,57] (Figure 2c).

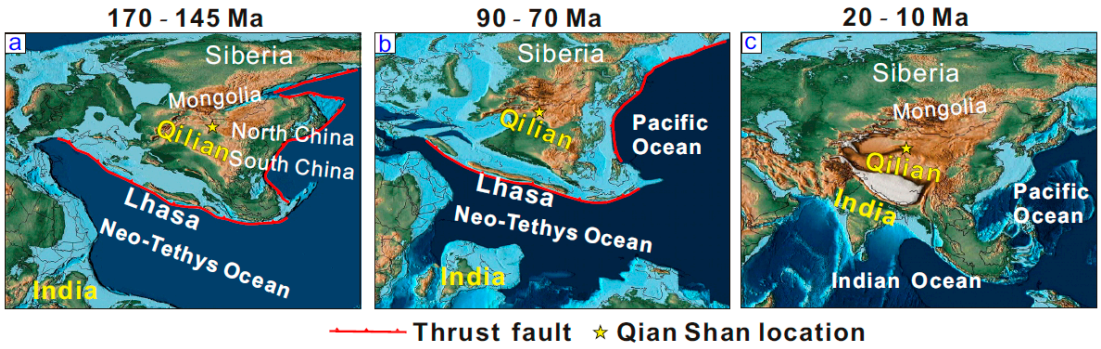

Figure 2. Reconstruction of the sea and land distribution map of East Asia from Neoproterozoic to Cenozoic. (**a**,**b**) The convergence of the Lhasa terrane and Asia caused the exhumation of the Qilian Shan in the Cretaceous. (**c**) The subduction of the Indian Plate under Asia led to multistage exhumation events in the Qilian Shan during the Cenozoic. The original maps were obtained from [58].

2.2. Daban Shan and Laji Shan

The eastern flank of the Central Qilian Shan includes the Daban Shan to the north and Laji Shan to the south (Figure 1c). The Daban Shan trends WNW for ~200 km with a width of ~50 km, is located at the northern margin of the Xining Basin, and is mainly composed of Early Paleozoic marine clastic deposits, volcanic rocks, and Devonian conglomerates that are unconformably covered by Mesozoic terrigenous clastic sediments [53] (Figure 1c). The Laji Shan extends E–W for ~200 km and is 10–30 km wide. This range separates the Guide Basin to the south from the Xining Basin to the north. During the Mesozoic and Cenozoic, the Daban Shan and Laji Shan were characterized by an episode of renewed and intense tectonic uplift [42,43,57]. The peaks of both Daban Shan and Laji Shan are at elevations averaging more than 4000 m above sea level [42].

2.3. Xining Basin

The area of the Xining Basin is ~100 × 80 km in size, and basin surface elevations mainly range between 2000 and 3000 m. Approximately E–W-oriented elongated thrust faults border the northern and southern margins of the Xining Basin along the northern and southern piedmonts of the Laji Shan and Daban Shan [59]. Cretaceous sediments primarily consist of sandstone and conglomerate, which were deposited along the two sides of the Huangshui River [60,61] (Figure 1c). Cenozoic strata in the Xining Basin can be divided into the Paleogene Xining and Neogene Guide groups. Neogene strata are almost devoid of gypsum and are characterized by massive brown to yellowish brown mudstones and siltstones intercalated with a conglomerate layer. The Xining Basin developed from a Late Jurassic–Early Cretaceous fault-related basin into a Paleogene flexural foreland basin [60] during intense basin deformation in the Miocene [42].

2.4. Huangshui River

The Huangshui River originates from the southern slope of the Datong Shan, has a total length of 370 km and a drainage area of 3200 km^2, and is an important tributary of the upper reaches of the Yellow River. It flows roughly W–E through the Xining Basin, has deeply incised the Precambrian to Mesozoic bedrock of the Xining Basin, and has formed up to 16 river terraces in the basin, with ages ranging from the Miocene to the Quaternary [61,62]. It merges with the Yellow River in the Gansu Province, China (Figure 1b).

Figure 3a shows that the detrital zircon ages of the three samples from the Huangshui River can be divided into five peaks with age ranges of 246–509, 899–1176, 1620–2089, and 2131–2610 Ma [22,23]. Characteristic age spectra of the Huangshui River samples resemble the detrital zircon age spectra of samples from the Central Qilian Shan [47] (Figure 3b). They also match the North Qilian Shan's source rock signatures [48,49] (Figure 3c), mainly because the Central and North Qilian terranes have similar evolutionary histories [26,50]. In addition, the data are broadly comparable to those from modern river and bedrock samples along the South Qilian Shan [44,61] (Figure 3d), Alxa Block [58] (Figure 3e), West Qinling [63] (Figure 3f), and upper reaches of the Yellow River [64] (Figure 3g). Age ranges of 700–900 Ma, 1800 Ma, and 2500 Ma were not obtained for the South Qilian Shan and West Qinling, whereas the samples from the Alxa Block lacked ages within the range of 200–500 Ma. Furthermore, the peak age composition of Yellow River samples differed from that of Huangshui River samples.

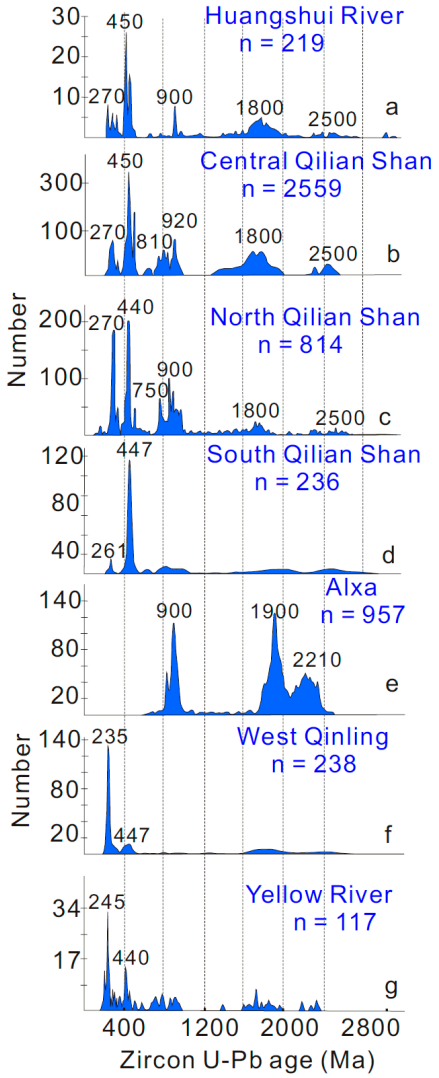

Figure 3. Compilation of detrital zircon U–Pb age spectra. Blue-shaded areas are kernel density estimates. (**a**) Modern river samples from the Huangshui River [22,23]. (**b**) Bedrock data for the Central Qilian Shan [24]. (**c**) Bedrock data for the North Qilian Shan [25,26]. (**d**) River data of the eastern section of the South Qilian Shan [27,28]. (**e**) Bedrock data for the Alxa Block [26]. (**f**) Integration of river sediment data from West Qinling [31]. (**g**) Modern river sediments in the upper reaches of the Yellow River [32].

3. Methods and Materials

We collected five sand samples (each ~3–5 kg) to conduct detrital ZFT and AFT dating on modern Huangshui River sediments (Figure 4). Sampling spots were chosen to obtain cooling age distributions from catchments at varying distances from upstream to downstream. The AFT and ZFT sampling information is presented in Table 1. Zircon and apatite mineral separation was conducted using standard separation techniques including jaw crushing and milling, sieving and washing, magnetic separators, and heavy-liquid separation. Each sample was hand-cleaned under a microscope to yield pure apatite and zircon grains suitable for FT analysis. Selected grains were mounted on Teflon and polished to reveal internal surfaces. All samples were dated using the 213 nm New Wave laser ablation system and inductively coupled plasma mass (Agilent 7800) spectrometry (LA-ICP-MS) at the Chronus Camp Research–Thermochronology Laboratory facilities in Brazil.

Figure 4. Photos of fluvial detrital sample collection in the Huangshui River Basin.

Table 1. Detrital apatite and zircon FT data of samples from the Huangshui River drainage.

Sample	GPS	AFT	ZFT
HY-1	101°18′14″ 36°40′55″	40	24
LD-1	102°22′22″ 36°28′58″	39	20
DTH-1	102°50′05″ 36°20′54″	28	21
HSH-1	102°55′04″ 36°18′21″	33	18
HSH-2	103°20′49″ 36°07′12″	13	25

The apatite grains were etched in NHO_3 (5.5 M) for 20 s at 21 °C to make the FTs visible [63]. AFTs were calibrated using the Durango standard (as age sample). The ^{238}U concentration was determined using uranium standards (Dur-2 and MT-7) with a <1.5% U variation [64]. The isotope concentration was carried out using a Neptune high-resolution multicollector ICP-MS coupled to a 193 Analyte Excite laser ablation system. Finally, NIST SRM 610 was analyzed together with age and uranium standards to check the LA-ICP-MS performance during analysis. The zircon grains were etched in a eutectic solution of KOH and NaOH at 228 °C for 18 h to reveal spontaneous FTs. Spontaneous FTs were counted after drying using a fully automated Leica DM6M microscope at a nominal magnification of 1000×. The ZFT ages were calibrated using Fish Canyon Tuff (FCT) as an age standard. Isotopes were measured using a quadrupole ICP-MS Agilent 7800 coupled to a UP213 nm New Wave Research laser ablation system [64]. The laser ablation spot size was selected to cover the maximum area of apatite and zircon grains in which FTs were measured. FT ages were calculated using the calibration method reported in Hurford and Green [65].

4. Results

In total, we obtained 152 and 106 new detrital AFT and ZFT single grain ages ranging from 627 to 0.5 Ma and 966 to 36.9 Ma, respectively (see Supplementary Materials Tables S1 and S2). The DensityPlotter program was used to decompose the age peaks. Due to the small number of zircon and apatite particles analyzed, which were located in the same small watershed, we combined them into one sample each.

Zircon U-Pb ages (≤1000 Ma) of the Huangshui River samples included the (1) Neoproterozoic age (19.48% of the grains), (2) Paleozoic age (75.38% of the grains), and (3) Mesozoic age (~5.12% of the grains) (Figure 5c). All other grains with FT ≤ U-Pb ages were considered to represent source rocks that cooled due to exhumation during the Mesozoic and

Cenozoic. AFT data, which provided information on the most recent thermal history and exhumation of source rocks, complemented the zircon U-Pb and ZFT data.

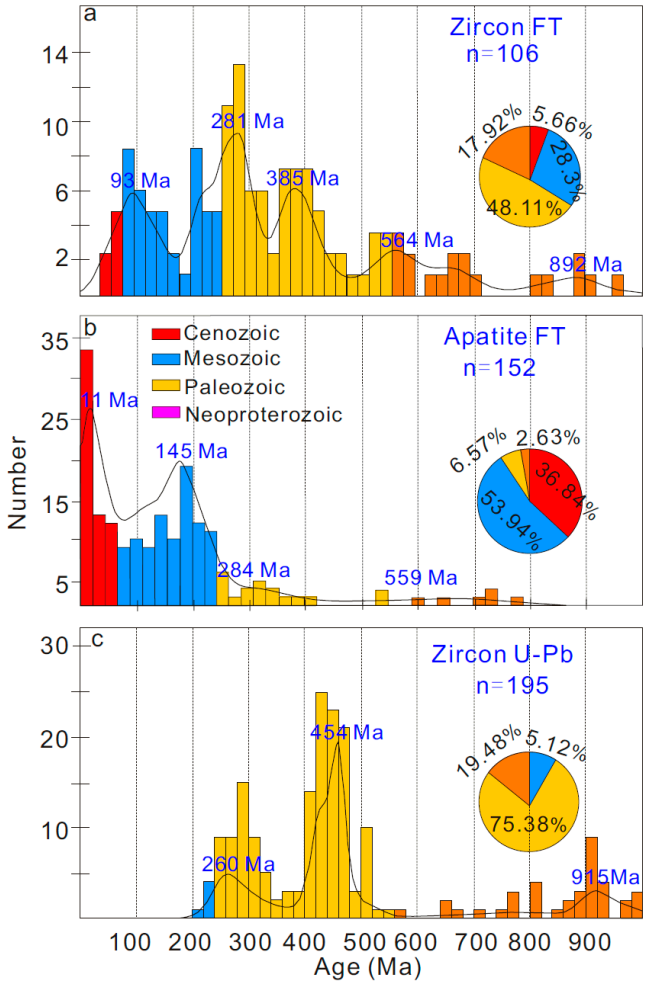

Figure 5. Zircon U–Pb age [22,23] (**a**), ZFT (**b**), and AFT (**c**) probability density plots for samples from the Huangshui River drainage. Plots were made with RadialPlotter from [66].

5. Discussion

Based on the assumption that detrital ZFT and AFT ages have not been reset by heating due to modern rivers and/or postdepositional burial in basins, the measured ages relate either to the formation age of a source area or its exhumation history [45,48,67–69]. The present-day thickness of the Xining Basin succession is limited (<3 km) and the regional thermal gradient is low (20–30 °C/km), suggesting low burial temperatures [43]. Based on this piece of evidence, significant postdepositional sample annealing can be ruled out. Detrital zircon U-Pb ages suggest that the fluvial sediments from the Huangshui River drainage were mainly sourced from the Central Qilian Shan [22,23]. Therefore, all samples yielded unreset cooling-age populations carrying a source area's magmatic or exhumation signal from the Xining Basin and both sides of the orogenic belts. However, since the U-Pb age analysis of the same zircon and apatite particles was not carried out, it is difficult to determine whether the particles with the same ZFT age and zircon U-Pb age recorded magmatic events. Among the samples from the Huangshui River, the youngest concordant U–Pb peak age obtained for detrital zircons was 226 Ma [23]. The magmatic events in the entire Qilian Shan almost completely ceased after the Mesozoic period [10,16], indicating that the Mesozoic–Cenozoic FT ages obtained for the Huangshui River samples were exhumation rather than magmatic signals (Figure 5). Therefore, we compared the modern Huangshui River detrital dataset with the bedrock AFT or ZFT ages of samples exposed

in the catchments and nearby areas, discussing the exhumation events along the Central Qilian Shan during the Mesozoic and Cenozoic periods.

5.1. The Mesozoic Exhumation

The AFT and ZFT peak ages ranging from 145 to 93 Ma belong to the Early Cretaceous and Late Cretaceous periods. Cretaceous (143 Ma and 97 Ma) AFT ages were obtained for the basement rocks of the Xining Basin [70] (Figure 6a(1)). The sedimentary record of the structural rejuvenation in the South Qilian Shan and North Qilian Shan preserved in the northeastern Qaidam Basin and Hexi Corridor indicates that intense tectonism occurred during the Early Cretaceous [54,56,71] (Figure 6a(2)). The sediment accumulation record, basin provenance, and angular unconformity between the strata provide evidence for rapid exhumation events within the Xining Basin during the Early Cretaceous and Late Cretaceous [57] (Figure 6a(3)). Detrital AFT data within the Xining Basin (94-77 Ma) [72] (Figure 6a(4)) and bedrock AFT data from the Daban Shan (88–70 Ma) [42] (Figure 6a(5)), and Laji Shan (93–85 Ma) [43] (Figure 6a(6)) demonstrate that rapid exhumation occurred during the Late Cretaceous. Therefore, the basements of the Xining Basin, Daban Shan, and Laji Shan are direct sources of the Cretaceous FT ages in our fluvial samples. This suggests that recycling of these sedimentary strata likely contributed zircon and apatite to modern fluvial sediments of the Huangshui River Basin. AFT thermal history modeling of samples from the western sectors of Central Qilian Shan revealed that rapid cooling occurred in the Cretaceous [18,20] (Figure 6a(7)), which was associated with the subduction of the Lhasa terrane along the southern margin of the Asian lithosphere [1,8]. This cooling event also occurred in the North [8,54,73] (Figure 6a(8)) and South Qilian Shan [17,74,75] (Figure 6a(9)). This indicates that the geomorphic framework of the northeastern margin of the Tibetan Plateau was initially established during the Mesozoic period (Figures 2a,b and 6b).

5.2. Cenozoic Exhumation

Our data confirm that the ongoing phase of exhumation of the Huangshui River drainage started at 11 Ma. This event may correspond to the rapid exhumation of the Laji Shan and Xining Basins during that time (10–8 Ma) [42,43,70] (Figure 6a(10)). The oldest fluvial terrace age was obtained in the upper reaches of the Huangshui River (10–6 Ma), corresponding to the Late Miocene exhumation of the Daban Shan and Laji Shan [61,62] (Figure 6a(11)). The bedrock apatite FT ages constrain the western parts of the Central Qilian Shan exhumed at 8 Ma [18] (Figure 6a(12)). This is consistent with the peak age of the detrital AFT (13–7 Ma) obtained for Danghe River samples [46] (Figure 6a(13)) as well as the broad bedrock AHe and AFT results of the North Qilian Shan (10–7 Ma [76,77]; Figure 6a(14)) and South Qilian Shan (7 Ma, [18,78]; Figure 6a(15)). An increase in exhumation and erosion in the Qilian Shan responded to the collision between the Indian and Eurasian continents during the Late Cenozoic [79,80]. Pollen records indicate the NE Tibetan Plateau increased rapidly to 3685 $\pm$ 87 m in the Late Miocene (~11 Ma) in the east, and to 3589 $\pm$ 62 m at ~7 Ma in the west [81]. Overall, our AFT data largely reflect an intense shallow-crust exhumation from the Huangshui River Basin, which is consistent with the topographic features of the mountain–river–basin distributions in the NE Tibetan Plateau that were gradually built from the Late Miocene (Figure 6b).

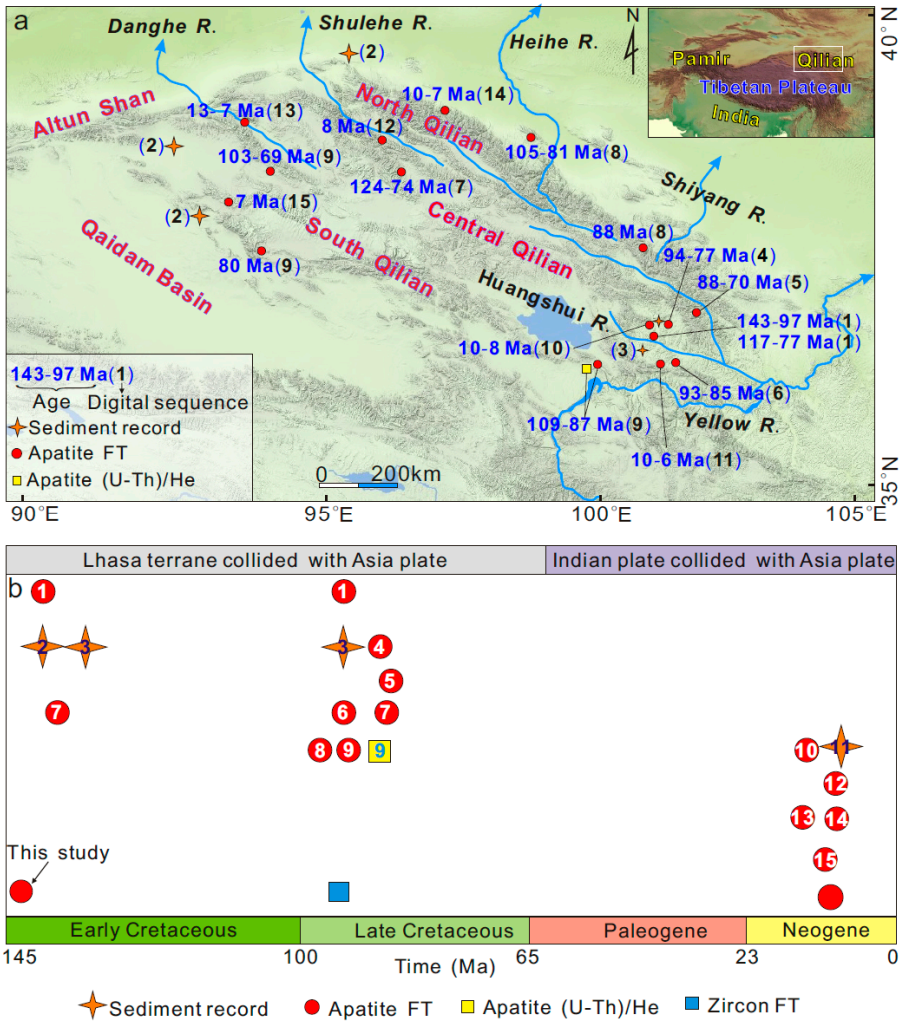

Figure 6. (**a**) Temporal distribution of tectonic events recorded in the Qilian Shan. (1): [70]; (2): [54,56,71]; (3): [57]; (4): [72]; (5): [42]; (6): [43]; (7): [18,20]; (8): [8,42,73]; (9): [17,74,75]; (10): [42,43,70]; (11): [61,62]; (12): [18]; (13): [46]; (14): [76,77]; (15): [18,78]. (**b**) Summary map of Mesozoic and Cenozoic low-temperature thermochronology and sedimentology in the Central Qilian Shan and its surrounding areas. The exhumation events of Mesozoic and Late Cenozoic are related to the collision of the Lhasa terrane and India plate with the Asia continent, respectively. The numbers in the figure correspond to those in Figure 6a.

6. Conclusions

Based on detrital ZFT and AFT analyses from the Huangshui River drainage, we derived information about both magmatic and exhumation cooling within the Central Qilian Shan:

(1) Mesozoic exhumations (145 and 93 Ma) in the Huangshui River drainage are related to the subduction of the Neo-Tethys Ocean. The geomorphic framework of the northeastern margin of the Tibetan Plateau was initially established during the Mesozoic period.

(2) The Central Qilian Shan responded to the collision between the Indian and Eurasian blocks during the Late Miocene (11 Ma), laying the foundation for the topographic features in the NE Tibetan Plateau.

Supplementary Materials: The following supporting information can be downloaded at: https://www.mdpi.com/article/10.3390/min13070890/s1, Table S1: Fission track results of detrital apatite in the Huangshui River; Table S2: Zircon fission track results from the Huangshui River.

Author Contributions: Conceptualization, X.L. and M.J.; methodology, X.L.; software, X.L.; validation, X.L., M.J. and F.C.; formal analysis, X.L.; investigation, X.L.; writing—original draft preparation, X.L.; writing—review and editing, X.L., M.J. and F.C. All authors have read and agreed to the published version of the manuscript.

Funding: This work was financially supported by the National Natural Science Foundation of China (grant 41972212).

Data Availability Statement: The data presented in this study are available on request from the corresponding author.

Acknowledgments: We thank Zhaoning Li for his help with the field sample collection.

Conflicts of Interest: The authors declare no conflict of interest.

References

1. Yin, A.; Harrison, T.M. Geologic evolution of the Himalayan-Tibetan orogen. *Annu. Rev. Earth Planet. Sci.* **2000**, *28*, 211–280. [CrossRef]
2. Liu-Zeng, J.; Tapponnier, P.; Gaudemer, Y.; Ding, L. Quantifying landscape differences across the Tibetan Plateau: Implications for topographic relief evolution. *J. Geophys. Res. Earth Surf.* **2008**, *113*, 1–26. [CrossRef]
3. Wang, C.; Zhao, X.; Liu, Z.; Lippert, P.C.; Graham, S.A.; Coe, R.S.; Li, Y. Constraints on the early uplift history of the Tibetan Plateau. *Proc. Natl. Acad. Sci. USA* **2008**, *105*, 4987–4992. [CrossRef]
4. Royden, L.H.; Burchfiel, B.C.; van der Hilst, R.D. The geological evolution of the Tibetan Plateau. *Science* **2008**, *321*, 1054–1058. [CrossRef] [PubMed]
5. Ding, L.; Kapp, P.; Cai, F.; Garzione, C.N.; Xiong, Z.; Wang, H.; Wang, C. Timing and mechanisms of Tibetan Plateau uplift. *Nat. Rev. Earth Environ.* **2022**, *3*, 652–667. [CrossRef]
6. Jolivet, M.; Cheng, F.; Zuza, A.V.; Guo, Z.; Dauteuil, O. Large-scale topography of the north Tibetan ranges as a proxy for contrasted crustal-scale deformation modes. *J. Geol. Soc.* **2022**, *179*, 1–15. [CrossRef]
7. Métivier, F.; Gaudemer, Y.; Tapponnier, P.; Meyer, B. Northeastward growth of the Tibet plateau deduced from balanced reconstruction of two depositional areas: The Qaidam and Hexi Corridor basins, China. *Tectonics* **1998**, *17*, 823–842. [CrossRef]
8. Tapponnier, P.; Xu, Z.; Roger, F.; Meyer, B.; Arnaud, N.; Wittlinger, G.; Jingsui, Y. Oblique stepwise rise and growth of the Tibet Plateau. *Science* **2001**, *294*, 1671–1677. [CrossRef]
9. Jolivet, M.; Brunel, M.; Seward, D.; Xu, Z.; Yang, J.; Roger, F.; Tapponnier, P.; Malavieille, J.; Arnaud, N.; Wu, C. Mesozoic and Cenozoic tectonics of the northern edge of the Tibetan plateau: Fission-track constraints. *Tectonophysics* **2001**, *343*, 111–134. [CrossRef]
10. Xia, L.Q.; Li, X.M.; Yu, J.Y.; Wang, G.Q. Mid-late Neoproterozoic to early Paleozoic volcanism and tectonic evolution of the Qilianshan, NW China. *GeoResJ* **2016**, *9*, 1–41. [CrossRef]
11. Zuza, A.V.; Wu, C.; Reith, R.C.; Yin, A.; Li, J.; Zhang, J.; Liu, W. Tectonic evolution of the Qilian Shan: An early Paleozoic orogen reactivated in the Cenozoic. *Geol. Soc. Am. Bull.* **2018**, *130*, 881–925. [CrossRef]
12. Li, B.; Chen, X.; Zuza, A.V.; Hu, D.; Ding, W.; Huang, P. Cenozoic cooling history of the North Qilian Shan, northern Tibetan Plateau, and the initiation of the Haiyuan fault: Constraints from apatite-and zircon-fission track thermochronology. *Tectonophysics* **2019**, *751*, 109–124. [CrossRef]
13. Cheng, F.; Garzione, C.N.; Mitra, G.; Jolivet, M.; Guo, Z.; Lu, H.; Wang, L. The interplay between climate and tectonics during the upward and outward growth of the Qilian Shan orogenic wedge, northern Tibetan Plateau. *Earth-Sci. Rev.* **2019**, *198*, 102945. [CrossRef]
14. Lin, X.; Jolivet, M.; Liu-Zeng, J.; Cheng, F.; Wu, Z.; Tian, Y.; Chen, J. The Formation of the North Qilian Shan through time: Clues from detrital zircon fission-track data from modern river sediments. *Geosciences* **2022**, *12*, 166. [CrossRef]
15. Xiao, W.; Windley, B.F.; Yong, Y.; Yan, Z.; Yuan, C.; Liu, C.; Li, J. Early Paleozoic to Devonian multiple-accretionary model for the Qilian Shan, NW China. *J. Asian Earth Sci.* **2009**, *35*, 323–333. [CrossRef]
16. Song, S.; Niu, Y.; Su, L.; Xia, X. Tectonics of the north Qilian orogen, NW China. *Gondwana Res.* **2013**, *23*, 1378–1401. [CrossRef]
17. Lin, X.; Jolivet, M.; Liu-Zeng, J.; Cheng, F.; Tian, Y.; Li, C. Mesozoic-Cenozoic cooling history of the Eastern Qinghai Nan Shan (NW China): Apatite low-temperature thermochronology constraints. *Palaeogeogr. Palaeoclimatol. Palaeoecol.* **2021**, *572*, 110416. [CrossRef]
18. Qi, B.; Hu, D.; Yang, X.; Zhang, Y.; Tan, C.; Zhang, P.; Feng, C. Apatite fission track evidence for the Cretaceous-Cenozoic cooling history of the Qilian Shan (NW China) and for stepwise northeastward growth of the northeastern Tibetan Plateau since early Eocene. *J. Asian Earth Sci.* **2016**, *124*, 28–41. [CrossRef]

19. Zuza, A.V.; Li, B.; Tremblay, M.M.; Chen, X.; Shuster, D.L.; Yin, A. Cenozoic development of the Northern Tibetan Plateau and the onset of thrust and strike-slip faulting: Constraints from apatite and zircon (U-Th)/He and fission-track thermochronometry. In *AGU Falling Meeting*; American Geophysical Union: Washington, DC, USA, 2016; p. T11A-2586.
20. Li, B.; Zuza, A.V.; Chen, X.; Wang, Z.Z.; Shao, Z.; Levy, D.A.; Sun, Y. Pre-cenozoic evolution of the northern Qilian Orogen from zircon geochronology: Framework for early growth of the northern Tibetan Plateau. *Palaeogeogr. Palaeoclimatol. Palaeoecol.* **2021**, *562*, 110091. [CrossRef]
21. Tong, K.; Li, Z.; Zhu, L.; Tao, G.; Zhang, Y.; Yang, W.; Zhang, J. Fold-and-thrust deformation of the hinterland of Qilian Shan, northeastern Tibetan Plateau since Mesozoic with implications for the plateau growth. *J. Asian Earth Sci.* **2020**, *198*, 104131. [CrossRef]
22. Cherniak, D.J.; Watson, E.B. Pb diffusion in zircon. *Chem. Geol.* **2001**, *172*, 5–24. [CrossRef]
23. Kang, H.; Chen, Y.L.; Li, D.P.; Bao, C.; Zhang, H.Z. Zircon U-Pb ages and Hf isotopic compositions of fluvial sediments from the Huangshui, Beichuan, and Xichuan rivers, Northwest China: Constraints on the formation and evolution history of the Central Qilian Block. *Geochem. J.* **2018**, *52*, 37–57. [CrossRef]
24. Yao, L. Detrital Zircon U-Pb Geochronology of the Xining Basin and Its Geological Implications in Cenozoic. Master's Thesis, Lanzhou University, Lanzhou, China, 2016; pp. 1–74, (In Chinese with English Abstract).
25. Zhao, X.; Liu, C.; Wang, J.; Zhao, Y.; Wang, L.; Zhang, Q. Detrital zircon U-Pb ages of Paleozoic sedimentary rocks from the eastern Hexi Corridor Belt (NW China): Provenance and geodynamic implications. *Sediment. Geol.* **2016**, *339*, 32–45. [CrossRef]
26. Zhang, J.; Zhang, B.; Zhao, H. Timing of amalgamation of the Alxa Block and the North China Block: Constraints based on detrital zircon U-Pb ages and sedimentologic and structural evidence. *Tectonophysics* **2016**, *668*, 65–81. [CrossRef]
27. Gong, H.; Zhao, H.; Xie, W.; Kang, W.; Zhang, R.; Yang, L.; Zhang, Y. Tectono-thermal events of the North Qilian Orogenic Belt, NW China: Constraints from detrital zircon U-Pb ages of Heihe River sediments. *J. Asian Earth Sci.* **2017**, *138*, 647–656. [CrossRef]
28. Kang, H.; Chen, Y.; Li, D.; Bao, C.; Chen, Y.; Xue, H. Detrital zircon record of rivers' sediments in the North Qilian Orogenic Belt: Implications of the tectonic evolution of the northeastern Tibetan Plateau. *Geol. J.* **2019**, *54*, 2208–2228. [CrossRef]
29. Song, B.; Zhang, K.; Hou, Y.; Ji, J.; Wang, J.; Yang, Y.; Shen, T. New insights into the provenance of Cenozoic strata in the Qaidam Basin, northern Tibet: Constraints from combined U-Pb dating of detrital zircons in recent and ancient fluvial sediments. *Palaeogeogr. Palaeoclimatol. Palaeoecol.* **2019**, *533*, 109254. [CrossRef]
30. Zhang, S.; Jian, X.; Pullen, A.; Fu, L.; Liang, H.; Hong, D.; Zhang, W. Tectono-magmatic events of the Qilian orogenic belt in northern Tibet: New insights from detrital zircon geochronology of river sands. *Int. Geol. Rev.* **2020**, *63*, 917–940. [CrossRef]
31. Lease, R.O.; Burbank, D.W.; Gehrels, G.E.; Wang, Z.; Yuan, D. Signatures of mountain building: Detrital zircon U/Pb ages from northeastern Tibet. *Geology* **2007**, *35*, 239–242. [CrossRef]
32. Liu, S. *Spatio-Temporal Evolution of Northeastern Tibetan Plateau: Integrated Provenance Study of the Guide, Lanzhou and Wushan-Tianshui Basins*; Lanzhou University: Lanzhou, China, 2015; pp. 1–135, (In Chinese with English Abstract).
33. Li, Z.; Wang, H.; Chen, X.; Zhang, E. *Geological Map of the People's Republic of China (Northwest) 1:1500000 Description*; Geological Publishing House: Beijing, China, 2019; pp. 1–188, (In Chinese with English Abstract).
34. Gehrels, G.E.; Yin, A.; Wang, X.F. Detrital-zircon geochronology of the northeastern Tibetan plateau. *Geol. Soc. Am. Bull.* **2003**, *115*, 881–896. [CrossRef]
35. Wu, C.; Zuza, A.V.; Yin, A.; Liu, C.; Reith, R.C.; Zhang, J.; Zhou, Z. Geochronology and geochemistry of Neoproterozoic granitoids in the central Qilian Shan of northern Tibet: Reconstructing the amalgamation processes and tectonic history of Asia. *Lithosphere* **2017**, *9*, 609–636. [CrossRef]
36. Li, Y.; Xiao, W.; Li, Z.; Wang, K.; Zheng, J.; Brouwer, F.M. Early Neoproterozoic magmatism in the Central Qilian block, NW China: Geochronological and petrogenetic constraints for Rodinia assembly. *Geol. Soc. Am. Bull.* **2020**, *132*, 2415–2431. [CrossRef]
37. Kang, H.; Chen, Y.; Xiong, J.; Li, D.; Xue, G. Tectonic affinity and significance of the Qilian Block: Evidence from river sediments in the Central Qilian Belt. *Geochemistry* **2023**, *83*, 125923. [CrossRef]
38. Donelick, R.A.; O'Sullivan, P.B.; Ketcham, R.A. Apatite fission-track analysis. *Rev. Mineral. Geochem.* **2005**, *58*, 49–94. [CrossRef]
39. Lease, R.O.; Burbank, D.W.; Clark, M.K.; Farley, K.A.; Zheng, D.; Zhang, H. Middle Miocene reorganization of deformation along the northeastern Tibetan Plateau. *Geology* **2011**, *39*, 359–362. [CrossRef]
40. Zheng, D.; Wang, W.; Wan, J.; Yuan, D.; Liu, C.; Zheng, W.; Zhang, P. Progressive northward growth of the northern Qilian Shan-Hexi Corridor (northeastern Tibet) during the Cenozoic. *Lithosphere* **2017**, *9*, 408–416. [CrossRef]
41. Yu, J.; Pang, J.; Wang, Y.; Zheng, D.; Liu, C.; Wang, W. Mid-Miocene uplift of the northern Qilian Shan as a result of the northward growth of the northern Tibetan Plateau. *Geosphere* **2019**, *15*, 423–432. [CrossRef]
42. Zhang, J.; Wang, Y.; Zhang, B.; Zhao, H. Evolution of the NE Qinghai-Tibetan Plateau, constrained by the apatite fission track ages of the mountain ranges around the Xining Basin in NW China. *J. Asian Earth Sci.* **2015**, *97*, 10–23. [CrossRef]
43. Wang, X.; Song, C.; Zattin, M.; He, P.; Song, A.; Li, J.; Wang, Q. Cenozoic pulsed deformation history of northeastern Tibetan Plateau reconstructed from fission-track thermochronology. *Tectonophysics* **2016**, *88*, 367–370. [CrossRef]
44. Wu, C.; Zuza, A.V.; Li, J.; Haproff, P.J.; Yin, A.; Chen, X.; Li, B. Late Mesozoic–Cenozoic cooling history of the northeastern Tibetan Plateau and its foreland derived from low-temperature thermochronology. *Geol. Soc. Am. Bull. Bull.* **2021**, *133*, 2393–2417. [CrossRef]
45. Garver, J.I.; Brandon, M.T.; Roden-Tice, M.; Kamp, P.J. Exhumation history of orogenic highlands determined by detrital fission-track thermochronology. *Geol. Soc. Lond. Spec. Publ.* **1999**, *154*, 283–304. [CrossRef]

46. Xu, Q.; Ji, J.; Zhao, W.; Sun, D.; Zhong, D.; Zhao, L. Late Cenozoic uplift-exhumation history of the Altyn Tagh and Qilian Mountains: Evidence from detrital apatite fission track thermochronology. *Chin. J. Geol.* **2015**, *50*, 1044–1067, (In Chinese with English Abstract).
47. Glotzbach, C.; Busschers, F.S.; Winsemann, J. Detrital thermochronology of Rhine, Elbe and Meuse river sediment (Central Europe): Implications for provenance, erosion and mineral fertility. *Int. J. Earth Sci.* **2018**, *107*, 459–479. [CrossRef]
48. Lin, X.; Tian, Y.; Donelick, R.A.; Liu-Zeng, J.; Cleber, S.J.; Wu, Q.; Li, Z. Mesozoic and Cenozoic tectonics of the northeastern edge of the Tibetan plateau: Evidence from modern river detrital apatite fission-track age constraints. *J. Asian Earth Sci.* **2019**, *170*, 84–95. [CrossRef]
49. Malusà, M.G.; Fitzgerald, P.G. Application of thermochronology to geologic problems: Bedrock and detrital approaches. In *Fission-Track Thermochronology and Its Application to Geology*; Springer: Cham, Switzerland, 2019; pp. 91–209.
50. Kirkland, C.L.; Barham, M.; Danišík, M. Find a match with triple-dating: Antarctic sub-ice zircon detritus on the modern shore of Western Australia. *Earth Planet. Sci. Lett.* **2020**, *531*, 115953. [CrossRef]
51. Carrapa, B.; Faiz bin Hassim, M.; Kapp, P.A.; DeCelles, P.G.; Gehrels, G. Tectonic and erosional history of southern Tibet recorded by detrital chronological signatures along the Yarlung River drainage. *Geol. Soc. Am. Bull.* **2017**, *129*, 570–581. [CrossRef]
52. Blayney, T.; Najman, Y.; Dupont-Nivet, G.; Carter, A.; Millar, I.; Garzanti, E.; Vezzoli, G. Indentation of the Pamirs with respect to the northern margin of Tibet: Constraints from the Tarim basin sedimentary record. *Tectonics* **2016**, *35*, 2345–2369. [CrossRef]
53. Gansu BGMR (Bureau of Geology and Mineral Resources). *Regional Geology Evolution of Gansu Province*; Geological Publishing House: Beijing, China, 1989; pp. 1–692, (In Chinese with English Abstract).
54. Ritts, B.D.; Biffi, U. Mesozoic northeast Qaidam basin: Response to contractional reactivation of the Qilian Shan, and implications for the extent of Mesozoic intracontinental deformation in central Asia. In *Memoirs-Geological Society of America*; Geological Society of America: Boulder, CO, USA, 2001; pp. 293–316.
55. George, A.D.; Marshallsea, S.J.; Wyrwoll, K.H.; Jie, C.; Yanchou, L. Miocene cooling in the northern Qilian Shan, northeastern margin of the Tibetan Plateau, revealed by apatite fission-track and vitrinite-reflectance analysis. *Geology* **2001**, *29*, 939–942. [CrossRef]
56. Cheng, F.; Garzione, C.; Jolivet, M.; Wang, W.; Dong, J.; Richter, F.; Guo, Z. Provenance analysis of the Yumen Basin and northern Qilian Shan: Implications for the pre-collisional paleogeography in the NE Tibetan Plateau and eastern termination of Altyn Tagh fault. *Gondwana Res.* **2019**, *65*, 156–171. [CrossRef]
57. Horton, B.; Dupont-Nivet, G.; Zhou, J.; Waanders, G.; Butler, R.; Wang, J. Mesozoic-Cenozoic evolution of the Xining-Minhe and Dangchang basins, northeastern Tibetan Plateau: Magnetostratigraphic and biostratigraphic results. *J. Geophys. Res. Solid Earth* **2004**, *109*, 1–35. [CrossRef]
58. Scotese, C.R. PALEOMAP PaleoAtlas for GPlates and the PaleoData Plotter Program, PALEOMAP Project. 2016. Available online: https://www.earthbyte.org/paleomap{-}{-}paleoatlas{-}{-}for{-}{-}gplates/ (accessed on 20 July 2021).
59. Fang, X.; Fang, Y.; Zan, J.; Zhang, W.; Song, C.; Appel, E. Cenozoic magnetostratigraphy of the Xining Basin, NE Tibetan Plateau, and its constraints on paleontological, sedimentological and tectonomorphological evolution. *Earth-Sci. Rev.* **2019**, *190*, 460–485. [CrossRef]
60. Dai, S.; Fang, X.; Dupont-Nivet, G.; Song, C.; Gao, J.; Krijgsman, W.; Zhang, W. Magnetostratigraphy of Cenozoic sediments from the Xining Basin: Tectonic implications for the northeastern Tibetan Plateau. *J. Geophys. Res. Solid Earth* **2006**, *111*, 1–19. [CrossRef]
61. Wang, X.; Lu, H.; Vandenberghe, J.; Zheng, S.; van Balen, R. Late Miocene uplift of the NE Tibetan Plateau inferred from basin filling, planation and fluvial terraces in the Huang Shui catchment. *Glob. Planet. Chang.* **2012**, *88*, 10–19. [CrossRef]
62. Lu, H.; Wang, X.; An, Z.; Miao, X.D.; Zhu, R.X.; Ma, H.Z.; Wang, X.Y. Geomorphologic evidence of phased uplift of the northeastern Qinghai-Tibet Plateau since 14 million years ago. *Sci. China Ser. D Earth Sci.* **2004**, *47*, 822–833. [CrossRef]
63. Carlson, W.D.; Donelick, R.A.; Ketcham, R.A. Variability of apatite fission-track annealing kinetics: I. Experimental results. *Am. Miner.* **1999**, *84*, 1213–1223. [CrossRef]
64. Soares, C.J.; Guedes, S.; Hadler, J.C.; Mertz-Kraus, R.; Zack, T. Novel calibrations for LA-ICP-MS-based fission-track thermochronology. *Phys. Chem. Miner.* **2014**, *41*, 65–73. [CrossRef]
65. Hurford, A.J.; Green, P.F. The zeta age calibration of fission-track dating. *Isot. Geosci.* **1983**, *1*, 285–317. [CrossRef]
66. Vermeesch, P. On the visualisation of detrital age distributions. *Chem. Geol.* **2012**, *312*, 190–194. [CrossRef]
67. Saylor, J.E.; Stockli, D.F.; Horton, B.K.; Nie, J.; Mora, A. Discriminating rapid exhumation from syndepositional volcanism using detrital zircon double dating: Implications for the tectonic history of the Eastern Cordillera, Colombia. *Geol. Soc. Am. Bull.* **2012**, *124*, 762–779. [CrossRef]
68. Bootes, N.; Enkelmann, E.; Lease, R. Late Miocene to Pleistocene source to sink record of exhumation and sediment routing in the gulf of Alaska from detrital zircon fission-track and U-Pb double dating. *Tectonics* **2019**, *38*, 2703–2726. [CrossRef]
69. Carter, A.; Bristow, C.S. Linking hinterland evolution and continental basin sedimentation by using detrital zircon thermochronology: A study of the Khorat Plateau Basin, eastern Thailand. *Basin Res.* **2003**, *15*, 271–285. [CrossRef]
70. Wang, Y.; Zhang, J.; Qi, W.; Guo, S. Exhumation history of the Xining Basin since the Mesozoic and its tectonic significance. *Acta Geol. Sin.-Engl. Ed.* **2015**, *89*, 145–162.
71. Wu, L.; Xiao, A.; Wang, L.; Shen, Z.; Zhou, S.; Chen, Y.; Guan, J. Late Jurassic–early Cretaceous northern Qaidam basin, NW China: Implications for the earliest Cretaceous intracontinental tectonism. *Cretac. Res.* **2011**, *32*, 552–564. [CrossRef]

72. Chen, L.; Song, C.; Wang, Y.; Fang, X.; Zhang, Y.; Zhang, J.; He, P. Mesozoic–Cenozoic Uplift/exhumation history of the Qilian Shan, NE Tibetan Plateau: Constraints from low-temperature thermochronology. *Front. Earth Sci.* **2021**, *9*, 760100. [CrossRef]
73. Chen, L.; Wang, Y.; He, P.; Song, C.; Meng, Q.; Feng, W.; Wang, X. Mesozoic-Cenozoic multistage tectonic deformation of the Qilian Shan constrained by detrital apatite fission track and zircon U-Pb geochronology in the Yumu Shan area. *Tectonophysics* **2022**, *822*, 229151. [CrossRef]
74. Jian, X.; Guan, P.; Zhang, W.; Liang, H.; Feng, F.; Fu, L. Late Cretaceous to early Eocene deformation in the northern Tibetan Plateau: Detrital apatite fission track evidence from northern Qaidam basin. *Gondwana Res.* **2018**, *60*, 94–104. [CrossRef]
75. He, P.; Song, C.; Wang, Y.; Zhao, Y.; Tan, Y.; Meng, Q.; Zhang, J. Cenozoic two-phase topographic growth of the northeastern Tibetan Plateau derived from two thermochronologic transects across the southern Qilian Shan thrust belt. *Tectonophysics* **2022**, *837*, 229432. [CrossRef]
76. Zheng, D.; Clark, M.K.; Zhang, P.; Zheng, W.; Farley, K.A. Erosion, fault initiation and topographic growth of the North Qilian Shan (northern Tibetan Plateau). *Geosphere* **2010**, *6*, 937–941. [CrossRef]
77. Shi, W.; Wang, F.; Yang, L.; Wu, L.; Zhang, W. Diachronous growth of the Altyn Tagh Mountains: Constraints on propagation of the northern Tibetan margin from (U-Th)/He dating. *J. Geophys. Res. Solid Earth* **2018**, *123*, 6000–6018. [CrossRef]
78. Pang, J.; Yu, J.; Zheng, D.; Wang, W.; Ma, Y.; Wang, Y.; Li, C.; Li, Y.; Wang, Y. Neogene Expansion of the Qilian Shan, North Tibet: Implications for the Dynamic Evolution of the Tibetan Plateau. *Tectonics* **2019**, *38*, 1018–1032. [CrossRef]
79. Lin, X.; Chen, H.; Wyrwoll, K.H.; Cheng, X. Commencing uplift of the Liupan Shan since 9.5 Ma: Evidences from the Sikouzi section at its east side. *J. Asian Earth Sci.* **2010**, *37*, 350–360. [CrossRef]
80. An, K.; Lin, X.; Wu, L.; Yang, R.; Chen, H.; Cheng, X.; Zhang, Y. An immediate response to the Indian-Eurasian collision along the northeastern Tibetan Plateau: Evidence from apatite fission track analysis in the Kuantan Shan-Hei Shan. *Tectonophysics* **2020**, *774*, 228278. [CrossRef]
81. Miao, Y.; Fang, X.; Sun, J.; Xiao, W.; Yang, Y.; Wang, X.; Utescher, T. A new biologic paleoaltimetry indicating Late Miocene rapid uplift of northern Tibet Plateau. *Science* **2022**, *378*, 1074–1079. [CrossRef]